Ground-state phase diagram of the SU(4) Heisenberg model on a plaquette lattice

Ryui Kaneko [1,*] Shimpei Goto [2,†] and Ippei Danshita [3,‡]
[1]*Physics Division, Sophia University, Chiyoda, Tokyo 102-8554, Japan*
[2]*College of Liberal Arts and Sciences, Tokyo Medical and Dental University, Ichikawa, Chiba 272-0827, Japan*
[3]*Department of Physics, Kindai University, Higashi-Osaka, Osaka 577-8502, Japan*

(Received 7 July 2024; accepted 12 August 2024; published 27 August 2024)

We investigate the ground state of the SU(4) Heisenberg model on a square lattice with spatial anisotropy on each plaquette bond using the tensor-network method based on infinite projected entangled pair states. We find that the SU(4) singlet ground state appears in the strongly anisotropic limit, whereas Néel and valence-bond crystal orders coexist in the nearly isotropic limit. By examining the intermediate parameter region, we identify a phase transition between these phases. The nature of the phase transition is likely to be of first order, and the transition point is estimated to be around $J'/J \approx 0.85(5)$, where J and J' are the interaction strengths of intra- and interplaquette bonds, respectively. We also calculate the anisotropy dependence of singlet correlations on a plaquette bond, which will be useful for future experiments of ultracold atoms in optical lattices.

DOI: 10.1103/PhysRevA.110.023326

I. INTRODUCTION

Lattice models with SU(N) symmetry, where $N > 2$, have recently attracted significant interest owing to the potential emergence of novel quantum states not found in the Hubbard and Heisenberg models with conventional SU(2) symmetry [1–6]. About a dozen years ago, such SU($N > 2$) systems were experimentally realized with ultracold atoms in optical lattices using ^{173}Yb [7], which is a fermionic isotope of alkaline-earth-like atoms. In contrast to other realistic platforms of SU($N > 2$) systems, such as antiferromagnets with coupled spin and orbital degrees of freedom [8–14], ultracold atoms in optical lattices are highly controllable.

Observing antiferromagnetic correlations in optical-lattice systems has long been a central issue in ultracold-atom experiments [15–19] and recent advances in cooling techniques have enabled the observation of antiferromagnetic correlations in SU(N) systems for large N [20]. Remarkably, antiferromagnetic correlations are more enhanced for SU(6) systems than for SU(2) systems, thanks to strong Pomeranchuk cooling effects [20]. This finding further stimulates research on quantum phase transitions caused by antiferromagnetic order in SU(N) systems with much larger N. On the other hand, antiferromagnetic correlations in SU(N) systems for rather small $N = 2$ and 4 can also be experimentally investigated on a cubic lattice with a spatial anisotropy in the hopping amplitudes favoring dimerization [18].

The physics of SU($N > 2$) systems is drastically different from that of SU(2) systems, even for a relatively small N, because of intertwined spin and orbital degrees of freedom. For example, the ground states of the SU(3) Heisenberg models exhibit a variety of exotic phases depending on the lattice geometry and the strength of the interactions. Spin nematic order emerges on a triangular lattice [21–23], unconventional stripe order appears on a square lattice [24], and plaquette valence-bond crystal (VBC) orders or related competing orders are found on honeycomb [25–27] and kagome [28,29] lattices.

However, the numerical investigation of quantum many-body states in SU(N) systems becomes significantly challenging when N increases [30–41]. Even for the SU(4) Heisenberg model on a simple lattice, the ground state is still under debate. For instance, cluster mean-field and spin-wave approximations have been used to investigate the ground state of the SU(4) Heisenberg model on a plaquette lattice, i.e., a square lattice with spatial anisotropy on plaquette bonds (see Fig. 1) [30,31]. These studies found that the SU(4) singlet ground state is favored in the strongly anisotropic regime. In the opposite limit, a prior tensor-network study suggested that the ground state should exhibit coexisting Néel and VBC order in the nearly isotropic region [32], although there would be many competing ground-state candidate states [33–37]. These findings imply a phase transition or other phases in the intermediate anisotropy region.

To understand the interplay between lattice spatial anisotropy and the spontaneous breaking of spin rotational and lattice translational symmetries in a simple SU(N) system, we investigate the ground states of the SU(4) Heisenberg model on a plaquette lattice using a two-dimensional tensor-network method based on infinite projected entangled pair states (iPEPS) [42–49] or infinite tensor product states [50–54]. We successfully reproduce the SU(4) singlet ground state in the strongly anisotropic limit and the Néel-VBC coexisting ground state in the nearly isotropic limit. By examining the intermediate parameter region, we identify a phase transition between these phases, which will be relevant to future experimental investigations.

*Contact author: ryuikaneko@sophia.ac.jp
†Contact author: goto.las@tmd.ac.jp
‡Contact author: danshita@phys.kindai.ac.jp

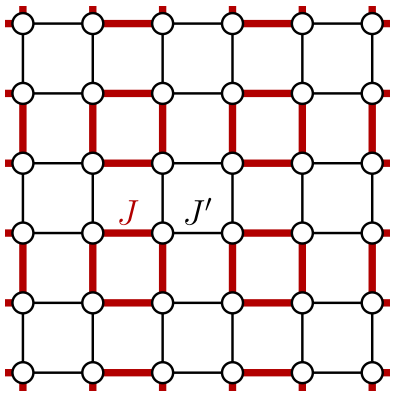

FIG. 1. Square lattice with spatial anisotropy on plaquette bonds. The interaction strength of intra- and interplaquette bonds is denoted by J (thick red lines) and J' (thin black lines), respectively. When $J'/J = 0$ and $J/J' = 0$, the system decouples into isolated four-site chains.

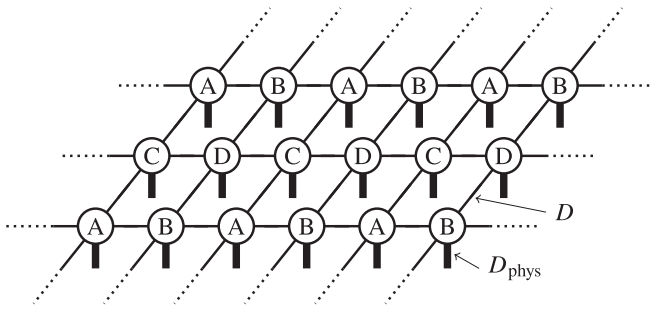

FIG. 2. Schematic representation of the iPEPS structure. Here we take a 2×2 sublattice structure as an example. The corresponding tensors A and B are rank-five tensors denoted by the circles. The tensors are connected with the physical (thick lines) and virtual (thin lines) bonds. The bond dimensions for the physical and virtual bond are denoted by $D_{\text{phys}}(= 4)$ and D, respectively.

This paper is organized as follows: In Sec. II, we introduce the SU(4) Heisenberg model on a plaquette lattice and the tensor-network method used in this study. In Sec. III, we present the results of the ground-state calculations and discuss the phase diagram of the model. We also calculate the anisotropy dependence of singlet correlations on plaquette bonds that can be measured in future experiments with ultracold atoms in optical lattices. Finally, we summarize our findings and discuss future prospects in Sec. IV. We set the reduced Planck constant as $\hbar = 1$ and a lattice constant as $a = 1$ throughout this paper.

II. MODEL AND METHOD

We consider the SU(4) antiferromagnetic Heisenberg model [32],

$$H_0 = J \sum_{\langle ij\rangle_{\text{intra}}} \hat{P}_{ij} + J' \sum_{\langle ij\rangle_{\text{inter}}} \hat{P}_{ij}, \tag{1}$$

on a plaquette lattice [30] (see Fig. 1). Here, $\hat{P}_{ij}$ is a transposition operator which exchanges flavors at sites i and j, namely, $\hat{P}_{ij}|\alpha_i\beta_j\rangle = |\beta_i\alpha_j\rangle$ ($\alpha_i, \beta_i \in \{0, 1, 2, 3\}$). The symbols $\langle ij\rangle_{\text{intra}}$ and $\langle ij\rangle_{\text{inter}}$ denote nearest-neighbor sites within a plaquette and between neighboring plaquettes, respectively. The interaction strengths for intra- and interbonds are denoted by J and J', respectively. Using the flavor-changing operator $\hat{S}^{\beta}_{\alpha}(i) = |\alpha_i\rangle\langle\beta_i|$, the Hamiltonian can be written as

$$H_0 = J \sum_{\langle ij\rangle_{\text{intra}}} \sum_{\alpha\beta} \hat{S}^{\beta}_{\alpha}(i)\hat{S}^{\alpha}_{\beta}(j) + J' \sum_{\langle ij\rangle_{\text{inter}}} \sum_{\alpha\beta} \hat{S}^{\beta}_{\alpha}(i)\hat{S}^{\alpha}_{\beta}(j). \tag{2}$$

Since the model with $J > J'$ and that with $J < J'$ are equivalent by interchanging the interaction strengths, we investigate the ground state of the model by controlling $J'/J \in [0, 1]$.

At $J'/J = 0$, the system decouples into four-site chains, and the ground state is an SU(4) singlet on each plaquette bond [30,31]. On the other hand, at $J'/J = 1$, the ground state is likely to be a Néel-VBC coexisting state [32]. Because both states are expected to have nonzero excitation gaps (of tetramer and dimer orders), these states would be robust against small perturbations. Then, the ground state would be a tetramerized state for $0 < J'/J \ll 1$, whereas it would still be the VBC state for $0 < 1 - J'/J \ll 1$. However, to the best of our knowledge, the nature of the ground state in the intermediate region ($0 < J'/J < 1$) has not been clarified yet.

One needs to take into account the effect of quantum fluctuations more accurately to investigate the stability of such crystal states beyond the mean-field-level approximations. To this end, we apply the two-dimensional tensor-network method based on iPEPS [42–54]. We illustrate the schematic structure of iPEPS in Fig. 2. The physical bond dimension is chosen as $D_{\text{phys}} = 4$, corresponding to the four flavors $\alpha = 0, 1, 2, 3$.

The ground-state candidate state for $J'/J \ll 1$, namely, the SU(4) singlet state, can be represented by the iPEPS with the bond dimension $D = 7$. On the other hand, for $J'/J \approx 1$, the ground state is expected to be a Néel-VBC coexisting state, which is found to be prepared after optimizing the dimerized initial state in iPEPS calculations for the bond dimension $D \geqslant 3$. For the details of the initial state preparation, see the Appendix.

We take the aforementioned SU(4) singlet and dimerized states as initial states and optimize these wave functions under several sublattice structures via imaginary-time evolution, as shown in Fig. 3. The 2×2 sublattice structure is suitable for representing the SU(4) singlet state, while the 4×1 sublattice structure is required for the Néel-VBC coexisting state. The 4×2 sublattice structure includes both 2×2 and 4×1 sublattice structures and allows for representing both ground-state candidate states and their coexistence, if any. To carefully take into account the effect of quantum fluctuations and investigate the possibility of other complicated ordered states, we also consider the 4×4 sublattice structure, which includes the 4×2 sublattice structure. Moreover, we use several random initial states when the SU(4) singlet and Néel-VBC coexisting states are competing for $D = 7$. After the optimization, we have always found that the random initial state converges to the Néel-VBC coexisting state. Therefore, we mainly optimize the SU(4) singlet and Néel-VBC coexisting states for bond dimensions $D > 7$.

We adopt the TeNeS library [55–57] and calculate the ground-state candidates up to $D = 12$ using the simple

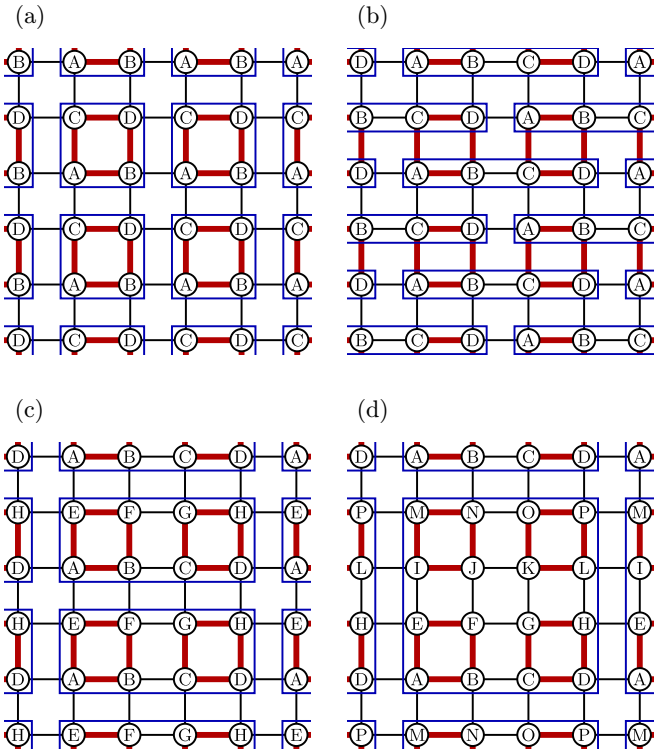

FIG. 3. Sublattice structures for the iPEPS calculation. We choose (a) 2×2 sublattice, (b) 4×1 sublattice, (c) 4×2 sublattice, and (d) 4×4 sublattice structures.

update algorithm [46,58]. We calculate physical quantities in the thermodynamic limit using the corner transfer matrix renormalization group (CTMRG) method [47–49,51,59–65]. To ensure the convergence of the physical quantities, we choose the bond dimension of the environment tensors as $\chi = \lfloor D^2/2 \rfloor$. The ground state at each J'/J for each bond dimension is determined by comparing the energies of candidate states and taking the lowest-energy state.

III. RESULTS

A. Energetics

We first investigate the ground-state candidate states of the model for several sublattice structures by fixing the bond dimension as $D = 7$ (see Fig. 4).

When the SU(4) singlet state is the initial state for the ground-state optimization process, the optimized state shows monotonically increasing energy as J'/J increases. The energy is nearly the same irrespective of the sublattice structure. This result indicates that the 2×2 sublattice structure is suitable for representing the SU(4) singletlike state, even for larger J'/J.

By contrast, when using the dimerized initial state, the energy of the optimized state exhibits a sublattice dependence significantly, in particular, for smaller J'/J. The energy obtained by the 4×1 sublattice structure is much higher than that obtained by the other sublattice structures, whereas the energies obtained by the 4×2 and 4×4 sublattice structures are nearly the same. This observation suggests that at least the 4×2 sublattice structure is required for effectively

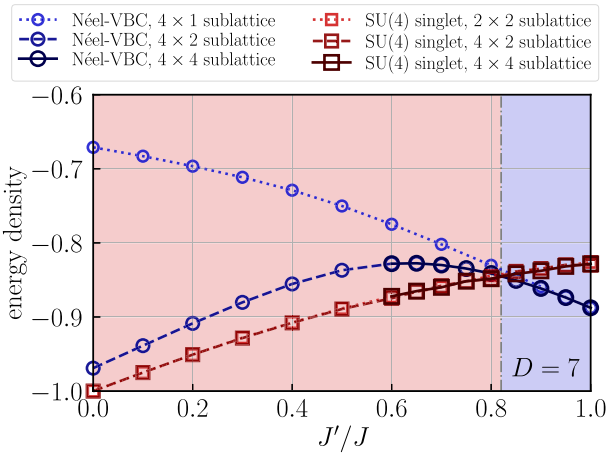

FIG. 4. Sublattice structure dependence of the energy per site as a function of J'/J for the bond dimension $D = 7$. Squares represent the SU(4) singlet state and circles represent the Néel-VBC coexisting state. The dash-dotted line represents the transition point.

representing the Néel-VBC coexistinglike state for smaller J'/J, while the energy is well converged by choosing the 4×2 sublattice structure.

As we will see in more detail later, for each finite bond dimension, the state obtained after optimizing the SU(4) singlet state still exhibits the SU(4) singletlike tetramer order and a small antiferromagnetic order (color order) even for larger J'/J [see Fig. 5(a)]. This state nearly keeps the $\mathbb{Z}_4$ lattice rotational symmetry. On the other hand, the state obtained after optimizing the dimerized state for 4×2 or 4×4 sublattice structures exhibits both dimer and antiferromagnetic order up to smaller J'/J [see Fig. 5(b)]; on one dimer bond, two out of four flavors are dominantly occupied, whereas on the other dimer bond, the other two flavors are dominantly occupied. This dimerized (Néel-VBC coexisting) state spontaneously breaks the lattice rotational symmetry.

We do not observe other ground-state candidate states as lowest-energy states in the intermediate parameter region ($0 < J'/J < 1$) up to the largest 4×4 sublattice structure at the bond dimension $D = 7$. Therefore, we mainly investigate the competition between the SU(4) singlet and dimerized

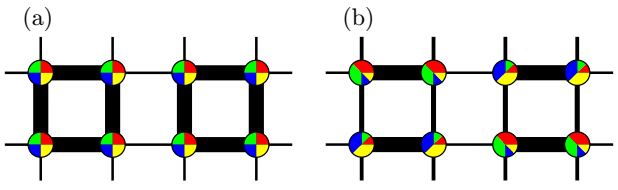

FIG. 5. Schematic pictures of the optimized states. (a) SU(4) singlet state for $J'/J \approx 0$. (b) Néel-VBC coexisting state for $J'/J \approx 1$. Each circle represents a site and the thickness of the line represents the strength of the bond correlation $\langle \hat{P}_{ij} \rangle$ between sites i and j. Four colors in each circle represent the four flavors $\alpha = 0, 1, 2, 3$, and the area of arc represents the ratio of the flavor occupation $\langle \hat{S}^{\alpha}_{\alpha}(i) \rangle$ at site i. In the absence of antiferromagnetic order (color order), $\langle \hat{S}^{\alpha}_{\alpha} \rangle$'s are equal for all flavors $\alpha = 0, 1, 2, 3$, and they become 1/4 since $\sum_{\alpha} \langle \hat{S}^{\alpha}_{\alpha} \rangle = 1$. Color order appears when they deviate from 1/4.

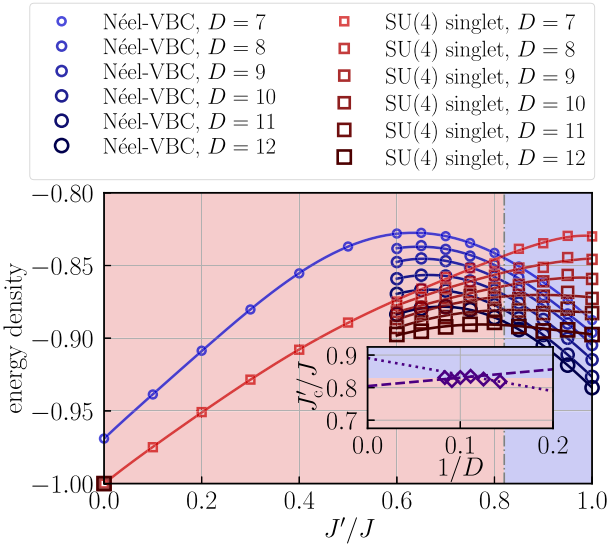

FIG. 6. Bond dimension dependence of the energy per site as a function of J'/J for the 4×2 sublattice structure. Squares represent the SU(4) singlet state and circles represent the Néel-VBC coexisting state. The energy obtained by a larger bond dimension is shown by a larger symbol. The dash-dotted line represents the transition point. Inset: The transition point as a function of the bond dimension.

states by increasing bond dimensions. Because the choice of the 4×2 and 4×4 sublattice structures does not significantly change the optimized states, hereafter we focus on the result on the 4×2 sublattice structure to reduce the computational cost.

We then investigate the energetics of these two ground-state candidate states for the 4×2 sublattice structure by varying the bond dimension D. As shown in Fig. 6, the energy of the SU(4) singlet state gradually decreases as the bond dimension increases. As the bond dimension increases, the J'/J dependence of energy becomes weaker for $J'/J \in [0.6, 1]$. In a similar manner, the energy of the Néel-VBC coexisting state moderately decreases as the bond dimension increases. For a fixed bond dimension, the energy of the Néel-VBC coexisting state signals a peak around $J'/J \approx 0.65$ and monotonically decreases as J'/J increases. Its curvature does not significantly change for all bond dimensions $D \geqslant 7$.

At each bond dimension, the energy of the SU(4) singlet state and that of the Néel-VBC coexisting state cross each other around $J'/J \approx 0.83$. With increasing bond dimensions, the transition point is gradually shifted to larger J'/J for $D \in [7, 9]$, while it is nearly converged for $D \geqslant 10$. We estimate the transition point via the linear extrapolation of the crossing points for smaller $D = 7, 8, 9$ and those for larger $D = 10, 11, 12$. From these results, we conclude that the transition point is around 0.85(5) (see the inset of Fig. 6).

Within the range of bond dimensions, $D \in [7, 12]$, that we have investigated, the nature of the transition is likely to be of first order. There are always metastable states of the SU(4) singlet state and the Néel-VBC coexisting state near the transition point, and a level crossing of these two states is observed for any bond dimensions. Although we cannot completely exclude the possibility of a continuous transition in the infinite bond dimension limit, investigating the nature of the transition

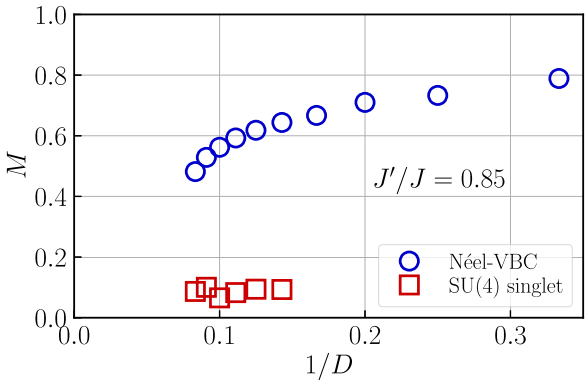

FIG. 7. Bond dimension dependence of the color order parameter for the SU(4) singlet (red squares) and Néel-VBC coexisting (blue circles) states in the 4×2 sublattice structure. The Néel-VBC coexisting state exhibits a sizable color order, whereas the SU(4) singlet state shows a small color order.

for larger bond dimensions is extremely challenging and we leave it for future study.

B. Physical properties

Having confirmed the phase transition between the SU(4) singlet and Néel-VBC coexisting states, we investigate the detailed physical properties that one would observe in experiments.

We calculate the color order parameter [32],

$$M = \frac{1}{N_{\text{sub}}} \sum_i \sum_\alpha \left| \langle \hat{S}^\alpha_\alpha(i) \rangle - \frac{1}{4} \right|, \tag{3}$$

where N_{sub} is the number of the sublattice sites. Here the summation is taken over all sublattice sites i and all flavors $\alpha = 0, 1, 2, 3$. In the ideal SU(4) singlet state at $J'/J = 0$, the color order parameter is zero because all flavors are equally occupied ($\langle \hat{S}^\alpha_\alpha \rangle = 1/4$). On the other hand, in the Néel-VBC coexisting state at $J'/J = 1$, the color order parameter is nonzero [32]. Note that in practical iPEPS calculations, the direction of the SU(4) symmetry breaking in the space of four flavors is explicitly chosen by the initial state preparation [32].

Figure 7 shows the color order parameter as a function of bond dimension D for the SU(4) singlet and Néel-VBC coexisting states near the transition point $J'/J \approx 0.85$. The Néel-VBC coexisting state exhibits a sizable color order and its value gradually decreases as the bond dimension increases. On the other hand, the SU(4) singlet state shows a much smaller color order than the Néel-VBC coexisting state. Although it is difficult to estimate color order parameters of both states in the infinite bond dimension limit, it is likely that the color order parameter for the SU(4) singlet state becomes nearly zero in the infinite bond dimension limit.

We also examine the bond energies,

$$E_b = \frac{1}{N_b} \sum_{\langle ij \rangle \in b} \langle \hat{P}_{ij} \rangle, \tag{4}$$

where the symbol $\sum_{\langle ij \rangle \in b}$ denotes the sum over bonds b, and N_b is the number of corresponding bonds in the unit cell. We

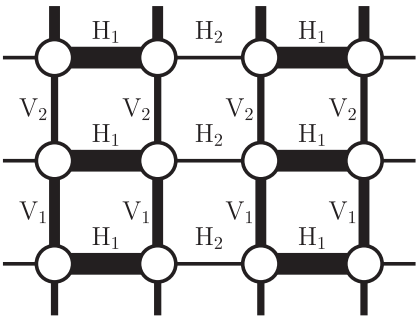

FIG. 8. Name of each bond. We calculate the bond energies along the H_1, H_2, V_1, and V_2 bonds in the 4×2 sublattice structure.

specifically focus on the bonds H_1, H_2, V_1, and V_2 (see Fig. 8) to distinguish the SU(4) singlet and Néel-VBC coexisting states.

Figure 9 shows the bond energies along the H_1, H_2, V_1, and V_2 bonds for the SU(4) singlet and Néel-VBC coexisting states near the transition point $J'/J \approx 0.85$. The SU(4) singlet state exhibits nearly the same bond energies along the H_1 and

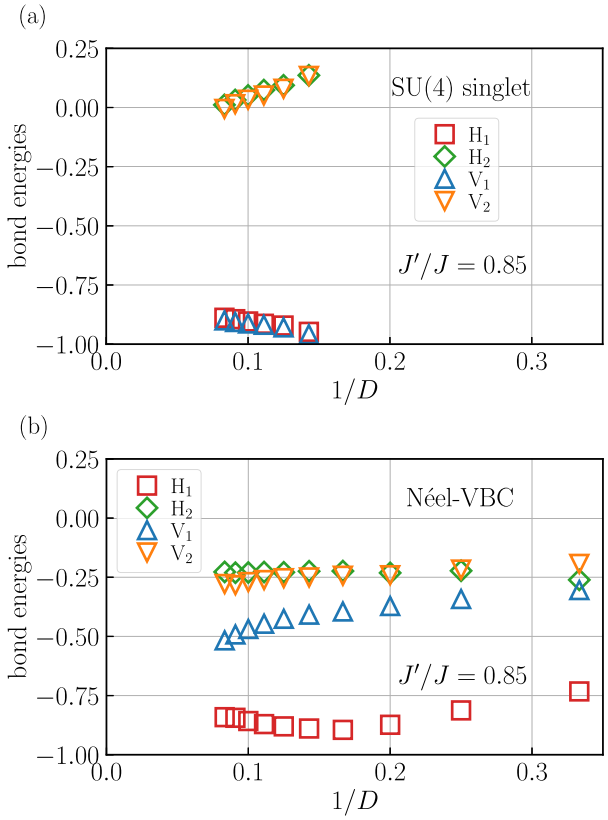

FIG. 9. Bond dimension dependence of each bond energy for (a) the SU(4) singlet and (b) Néel-VBC coexisting states in the 4×2 sublattice structure. The bond energies are calculated along the H_1 (red squares), H_2 (green diamonds), V_1 (blue up-pointing triangles), and V_2 (orange down-pointing triangles) bonds. Even near the transition point $J'/J \approx 0.85$, the SU(4) singlet state satisfies $E_{H_1} \approx E_{V_1}$ and $E_{H_2} \approx E_{V_2}$, indicating the stable tetramerization. On the other hand, the Néel-VBC coexisting state exhibits the stable dimerization ($|E_{H_1}| > |E_{V_1}|, |E_{V_2}|, |E_{H_2}|$).

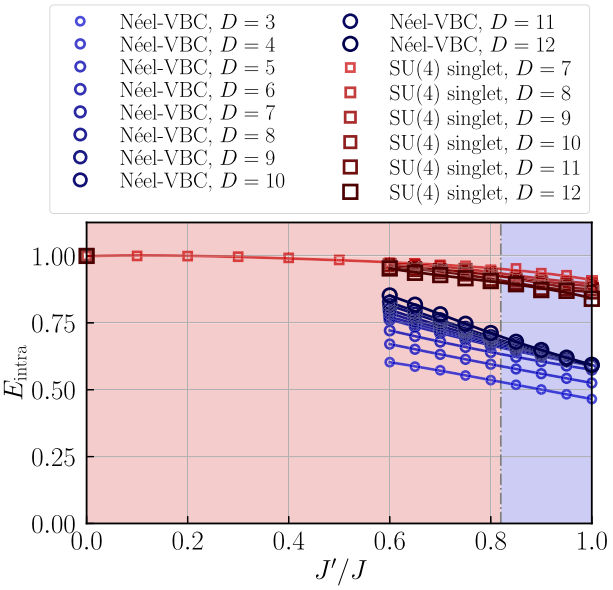

FIG. 10. Anisotropy dependence of the bond energy on intraplaquette bonds for the 4×2 sublattice structure. Squares represent the SU(4) singlet state and circles represent the Néel-VBC coexisting state. The data obtained by a larger bond dimension are shown by a larger symbol. The dash-dotted line represents the transition point.

V_1, as well as nearly the same bond energies along the H_2 and V_2 bonds. This observation indicates that the SU(4) singlet state satisfies the stable tetramerization even near the transition point. Considering the fact that the SU(4) singlet state shows a nearly zero color order parameter, the ground state at $J'/J = 0$ appears to persist rather close to the isotropic limit $J'/J = 1$. On the other hand, the Néel-VBC coexisting state exhibits the stable dimerization ($|E_{H_1}| > |E_{V_1}|, |E_{V_2}|, |E_{H_2}|$). Remarkably, the bond energy along the V_1 bond is somewhere in between the largest bond energy along the H_1 bond and the smallest bond energy along the H_2 and V_2 bonds. In this sense, the Néel-VBC coexisting state gradually becomes the SU(4) singletlike state as J'/J decreases, although the color order parameter is nonzero and the lattice rotational symmetry is not fully recovered even at $J'/J = 0$ (not shown).

In SU(N) systems realized with ultracold atoms in optical lattices, one multimerizes the system along specific directions and observes an excess of singlets compared with triplets. By optically inducing a singlet-triplet oscillation [66], one can measure antiferromagnetic correlations [7,18,20]. To directly compare with such quantities accessible in experiments, we also calculate the bond energy only on intraplaquette bonds, which is defined as

$$E_{\text{intra}} = -\frac{1}{N_{\text{intrabond}}} \sum_{\langle ij \rangle_{\text{intra}}} \langle \hat{P}_{ij} \rangle = -\frac{E_{H_1} + E_{V_1}}{2}. \quad (5)$$

Here, $N_{\text{intrabond}}$ is the number of the intraplaquette bonds in the unit cell, and $N_{\text{intrabond}} = 8$ is for the 4×2 sublattice structure. It takes the value $E_{\text{intra}} = 1$ when the ground state is the SU(4) singlet state and, in general, measures the intensity of singlet correlations along the intraplaquette bonds.

We illustrate the anisotropy dependence of the bond energy on intraplaquette bonds as shown in Fig. 10. For a smaller

$J'/J \lesssim 0.83$, the ground state is the SU(4) singlet state and its bond energy is nearly saturated. This observation indicates that the stable tetramerization persists even for large J'/J close to the isotropic limit. For $J'/J \gtrsim 0.83$, the ground state becomes the Néel-VBC coexisting state and its bond energy is smaller than that of the SU(4) singlet state. As J'/J increases, the dimerization becomes stronger and the bond energy along the vertical bonds V_1 and that along the horizontal bond H_1 deviate from each other. The bond energy on intraplaquette bonds jumps around $J'/J \approx 0.83$, which might be detected in future experiments of ultracold atoms in optical lattices by utilizing singlet-triplet oscillations.

IV. SUMMARY AND OUTLOOK

In conclusion, we investigated the ground state of the SU(4) Heisenberg model on a plaquette lattice using the two-dimensional tensor-network method based on iPEPS. We analyzed two competing ground-state candidate states: the SU(4) singlet state and the Néel-VBC coexisting state. We showed that the former is the ground state in the strongly anisotropic limit, whereas the latter is the ground state in the nearly isotropic limit. By examining the intermediate parameter region, we identified a first-order phase transition between these phases. The transition point was estimated to be around $J'/J \approx 0.85(5)$, where J and J' are the interaction strengths of the intra- and interplaquette bonds, respectively.

Compared to the SU(2) model on a plaquette lattice, where the transition between the s-wave resonating-valence-bond state [67,68] and the Néel state takes place around 0.5485(2) [69], the SU(4) singlet ground state persists in the nearly isotropic limit. Indeed, exact diagonalization calculations for 4×4 sites give the SU(4) singletlike (plaquette) ground state on the isotropic square lattice [34], and such a state seems to be a low-energy state (but not the ground state) in the thermodynamic limit. This observation suggests that the spontaneous multimerization is more easily realized in SU(N) systems with very large N. In this sense, investigating the ground state of the SU(N) model on an isotropic square lattice for larger N will be an interesting future study.

In ultracold-atom experiments, one can measure antiferromagnetic correlations by optically inducing a singlet-triplet oscillation [66]. We calculated the anisotropy dependence of such correlations and found that it is nearly saturated even for large $J'/J \lesssim 0.85(5)$. It eventually jumps around the transition point and takes a relatively large value (but smaller than the saturated value) near the isotropic limit. These results will be useful for future experiments with ultracold atoms in optical lattices.

The effects of magnetic field and other perturbations will enrich the phase diagram of the model [30,31]. It is also interesting to investigate the ground state of the SU(4) model in such situations using the tensor-network method, which we leave for future study.

ACKNOWLEDGMENTS

The authors acknowledge fruitful discussions with Kentaro Honda, Daichi Kagamihara, Mathias Mikkelsen, Yuki Miyazaki, Shintaro Taie, Yoshiro Takahashi, Yosuke Takasu, Takuto Tsuno, and Daisuke Yamamoto. This work was supported by JSPS KAKENHI (Grant No. JP24H00973), MEXT KAKENHI, Grant-in-Aid for Transformative Research Area (Grants No. JP22H05111 and No. JP22H05114), JST FOREST (Grant No. JPMJFR202T), and MEXT Q-LEAP (Grant No. JPMXS0118069021). The numerical computations were performed on computers at the Yukawa Institute Computer Facility, Kyoto University and on computers at the Supercomputer Center, the Institute for Solid State Physics, the University of Tokyo.

APPENDIX: INITIAL STATE PREPARATION

In this section, we describe the initial state preparation for the iPEPS calculation. We specifically focus on the SU(4) singlet initial state and the dimerized initial state for the SU(4) Heisenberg model on a plaquette lattice.

1. Tensor-network representation of the SU(N) singlet state

Here we show that the SU(N) singlet state on an N-site chain can be described by the matrix product state (MPS) with the maximum virtual bond dimension $D_{\mathrm{MPS}} = \binom{N}{\lfloor N/2 \rfloor}$. For simplicity, let us focus on the SU($N = 3$) case, where the required maximum bond dimension is $D_{\mathrm{MPS}} = 3$. The singlet state is given by

$$|\psi\rangle \propto |012\rangle - |021\rangle - |102\rangle + |120\rangle + |201\rangle - |210\rangle \tag{A1}$$

$$= \sum_{i,j,k \in \{0,1,2\}} \epsilon_{i,j,k} |ijk\rangle, \tag{A2}$$

where $\epsilon_{i,j,k}$ denotes the Levi-Civita symbol. We will construct the MPS at each site (0, 1, and 2) in a way such that the trace of the product of the MPSs gives $\epsilon_{i,j,k}$.

To this end, we first prepare the power set of a set $S = \{0, 1, 2, \ldots, N-1\}$. For each subset containing $n(\in \{0, 1, 2, \ldots, N-1, N\})$ elements, we define the function ind$(\cdot)$ as shown in Table I. For example, to generate the subset for #set $= 2$, we select the smallest number 0 as the first element and then select the second smallest number 1 as the second element, which gives the subset $\{0, 1\}$. To avoid double counting, we enumerate the subsets in ascending order so that the right element is always larger than the left element. We assign the index 0 to this subset $\{0, 1\}$. Next, we

TABLE I. Power set of a set $S = \{0, 1, 2, \ldots, N-1\}$ for $N = 3$ and the corresponding index for each subset. The symbol # denotes the number of elements in each set. The index of the left or right virtual bond takes the value of ind(set).

set	#set	ind(set)
{}	0	0
{0}	1	0
{1}	1	1
{2}	1	2
{0, 1}	2	0
{0, 2}	2	1
{1, 2}	2	2
{0, 1, 2}	3	0

TABLE II. Nonzero tensor elements of the iPEPS representation of the SU(4) singlet state. The sublattice sites A, B, C, and D of the 2×2 sublattice structure defined in Fig. 3(a) are represented by the site index $(x, y) = (0, 0)$, (1,0), (0,1), and (1,1), respectively. The index of the left, top, right, and bottom virtual bonds takes the value $0, 1, \ldots, 6(= D - 1)$ with $D = 7$. The index of the physical bond (color) 0,1,2,3 corresponds to the four flavors of the SU(4) model. The value of the tensor $T_{\text{left,top,right,bottom,color}}$ is given by the appropriate sign. This iPEPS representation on a plaquette corresponds to the MPS representation on a four-site chain (connecting sites in order of A, B, D, and C) with the bond dimension $D_{\text{MPS}} = 6$ (corresponding to the index of virtual bonds $1, 2, \ldots, 6$).

Site	Left	Top	Right	Bottom	Color	Value
(0,0)	0	1	1	0	0	+1
(0,0)	0	1	2	0	1	+1
(0,0)	0	1	3	0	2	+1
(0,0)	0	1	4	0	3	+1
(1,0)	1	1	0	0	1	+1
(1,0)	1	2	0	0	2	+1
(1,0)	1	3	0	0	3	+1
(1,0)	2	1	0	0	0	−1
(1,0)	2	4	0	0	2	+1
(1,0)	2	5	0	0	3	+1
(1,0)	3	2	0	0	0	−1
(1,0)	3	4	0	0	1	−1
(1,0)	3	6	0	0	3	+1
(1,0)	4	3	0	0	0	−1
(1,0)	4	5	0	0	1	−1
(1,0)	4	6	0	0	2	−1
(1,1)	1	0	0	1	2	+1
(1,1)	2	0	0	1	3	+1
(1,1)	1	0	0	2	1	−1
(1,1)	3	0	0	2	3	+1
(1,1)	2	0	0	3	1	−1
(1,1)	3	0	0	3	2	−1
(1,1)	1	0	0	4	0	+1
(1,1)	4	0	0	4	3	+1
(1,1)	2	0	0	5	0	+1
(1,1)	4	0	0	5	2	−1
(1,1)	3	0	0	6	0	+1
(1,1)	4	0	0	6	1	+1
(0,1)	0	0	1	1	3	+1
(0,1)	0	0	2	1	2	−1
(0,1)	0	0	3	1	1	+1
(0,1)	0	0	4	1	0	−1

fix the first element 0 and select the next smallest number 2, which gives the subset $\{0, 2\}$. The index of this subset is 1. We repeat this procedure by fixing the first element 1 and increasing the remaining elements until the last element $N - 1$ is selected. We then select the second smallest number 1 as the first element and select the next smallest number 2 as the second element, which gives the subset $\{1, 2\}$. The index of this subset is 2. Again, we fix the first element and increase the remaining elements until the last element $N - 1$ is selected. We repeat this procedure until we obtain the last subset $\{N - n, \ldots, N - 3, N - 2, N - 1\}$ for #set $= n$ in general. (For $N = 3$ and $n = 2$, the subset $\{1, 2\}$ is the last subset.) Then, the maximum index is given by $\binom{N}{n} - 1$.

TABLE III. Nonzero tensor elements of the iPEPS representation of the dimerized state. The sublattice sites A, B, C, and D of the 4×1 sublattice structure defined in Fig. 3(b) are represented by the site index $(x, y) = (0, 0)$, (1,0), (2,0), and (3,0), respectively. The index of the left, top, right, and bottom virtual bonds takes the value $0, 1, 2(= D - 1)$ with $D = 3$. The index of the physical bond (color) 0,1,2,3 corresponds to the four flavors of the SU(4) model. The value of the tensor $T_{\text{left,top,right,bottom,color}}$ is given by the appropriate sign.

Site	Left	Top	Right	Bottom	Color	Value
(0,0)	0	0	1	0	0	+1
(0,0)	0	0	2	0	1	+1
(1,0)	1	0	0	0	1	+1
(1,0)	2	0	0	0	0	−1
(2,0)	0	0	1	0	2	+1
(2,0)	0	0	2	0	3	+1
(3,0)	1	0	0	0	3	+1
(3,0)	2	0	0	0	2	−1

The index ind(set) will be used to label the left and right virtual bonds. On the other hand, the physical bond takes the flavor $s = 0$, 1, or 2, and so does its index. This choice

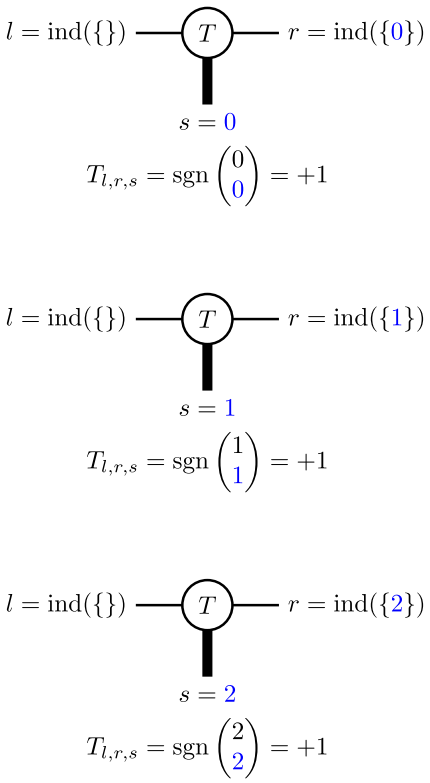

FIG. 11. Nonzero MPS elements at site 0 for the SU($N = 3$) singlet state. The index of the left or right virtual bond takes the value of ind(set), which is defined in Table I. The value of the tensor $T_{l,r,s}$ is given by the sign of the permutation corresponding to a sequence $(s_0, s_1, \ldots, s_{\#\text{set}_l - 1}, s)$, whose order matters. The sequence is generated from the set at the left bond ($\text{set}_l = \{s_0, s_1, \ldots, s_{\#\text{set}_l - 1}\}$) and the color of the physical bond ($s = 0$, 1, or 2). At site 0, the set at the left bond is the empty set and that at the right bond is a size-1 subset.

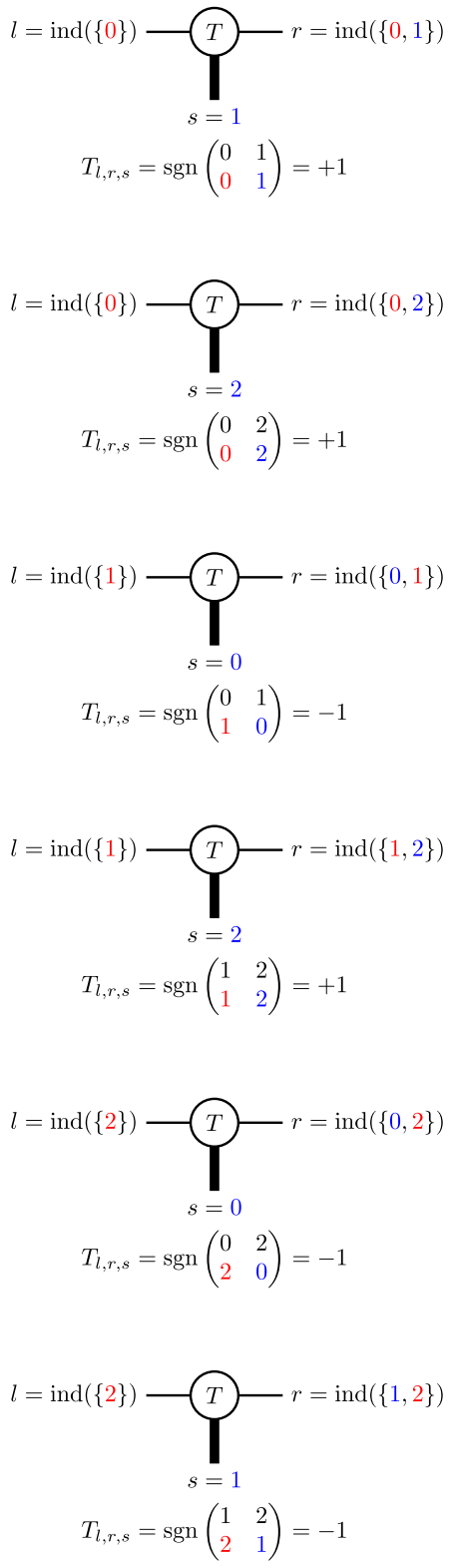

FIG. 12. Nonzero MPS elements at site 1 for the SU($N = 3$) singlet state. The notation is the same as that in Fig. 11.

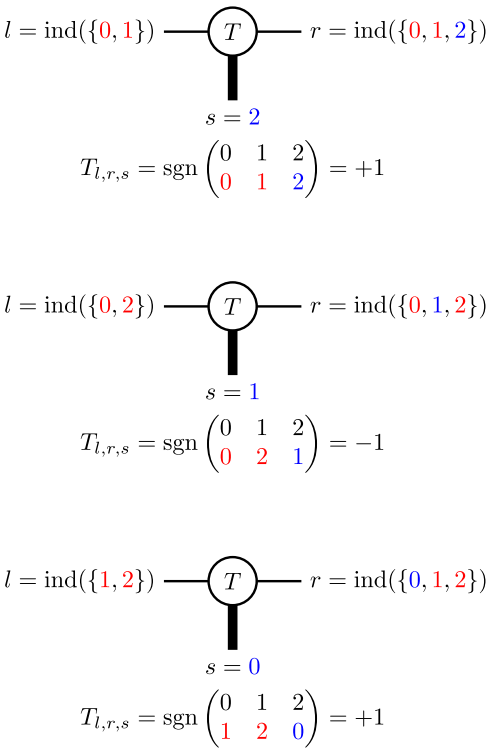

FIG. 13. Nonzero MPS elements at site 2 for the SU($N = 3$) singlet state. The notation is the same as that in Fig. 11.

corresponds to providing s in ascending order from the elements of the set {0, 1, 2} satisfying #set = 1. As we will see below, the element of the tensor $T_{l,r,s}$ is chosen as the sign of the permutation corresponding to a certain sequence, whose order matters, that is generated from the set at the left bond and the color at the physical bond.

Next, we construct the MPS at site 0 (see Fig. 11). For the left bond, we choose an empty set $\mathrm{set}_l = \{\}$. The maximum dimension of the left bond is 1 at site 0, and the index of the left bond can only take the value $l = 0$. For the physical bond, the color can take the value $s = 0$, 1, or $2(= N - 1)$. For the right bond, we choose a set depending on the color at the physical bond, i.e., $\mathrm{set}_r = \{s\}$. The index of the right bond takes the value $r = \mathrm{ind}(\mathrm{set}_r) = s$ and the maximum dimension of the right bond is 3 at site 0. The value of the tensor element $T_{l,r,s}$ at site 0 will be equivalent to $T_{0,s,s}$. It is chosen as $+1$ for all s because the permutation corresponding to the sequence (s) is the identity.

Then, we construct the MPS at site 1 (see Fig. 12). For the left bond, we choose a set corresponding to that for the right bond at site 0. It is given as $\mathrm{set}_l = \{s_0\}$, with $s_0 = 0$, 1, or 2 being the color of the physical bond at site 0. The maximum dimension of the left bond is 3 at site 1, and the index of the left bond takes the value $l = 0$, 1, or 2. For the right bond, we prepare a set $\mathrm{set}_r = \{s_0, s\}$, which is constructed from the element of $\mathrm{set}_l = \{s_0\}$ and the color at the physical bond s at site 1. Since the index of the right bond takes the value $r = 0$, 1, or 2, the maximum dimension of the right bond is 3 at site 1. The tensor element $T_{l,r,s}$ at site 1 is nonzero only when $\#\mathrm{set}_r = 2$. It will be obtained by the sign of the permutation corresponding to a sequence (s_0, s), whose order matters; it is positive (negative) if the parity is even (odd). For example, when we have a sequence (0,1), we generate the permutation $\sigma = \binom{0\ \ 1}{0\ \ 1}$ and assign its sign $\mathrm{sgn}(\sigma) = +1$ to $T_{l,r,s}$. On the

other hand, when we have a sequence (1,0), we generate the permutation $\sigma = \left(\begin{smallmatrix} 0 & 1 \\ 1 & 0 \end{smallmatrix}\right)$ and assign its sign $\mathrm{sgn}(\sigma) = -1$ to $T_{l,r,s}$.

Finally, we construct the MPS at site 2 (see Fig. 13). For the left bond, we choose a set corresponding to that for the right bond at site 1. It is given as $\mathrm{set}_l = \{s_0, s_1\} = \{0, 1\}, \{0, 2\}$, or $\{1, 2\}$. The maximum dimension of the left bond is 3 at site 2, and the index of the left bond takes the value $l = 0$, 1, or 2. For the right bond, we prepare a set $\mathrm{set}_r = \{s_0, s_1, s\}$, which is constructed from the element of $\mathrm{set}_l = \{s_0, s_1\}$ and the color at the physical bond s at site 2. This actually becomes $\mathrm{set}_r \equiv \{0, 1, 2\}$, and then the index of the right bond only takes the value $r = \mathrm{ind}(\{0, 1, 2\}) = 0$. The corresponding maximum dimension of the right bond is 1 at site 2. This dimension 1 is consistent with that of the left bond at site 0, which allows us to safely calculate the trace of product of three tensors. The tensor element $T_{l,r,s}$ at site 2 is nonzero only when $\#\mathrm{set}_r = 3$, and it will again be obtained by the sign of the permutation corresponding to a sequence (s_0, s_1, s).

From these three tensors $T^{(i)}_{l,r,s}$ at sites $i = 0$, 1, and 2, we evaluate the trace of product of them. Easy calculations yield

$$\mathrm{Tr}_{i_0,i_1,i_2} T^{(0)}_{i_0,i_1,s_0} T^{(1)}_{i_1,i_2,s_1} T^{(2)}_{i_2,i_0,s_2} = \epsilon_{s_0,s_1,s_2}. \tag{A3}$$

Here the virtual bonds take the value $i_0 = 0$, $i_1, i_2 \in \{0, 1, 2\}$, and the physical bond takes the value $s_0, s_1, s_2 \in \{0, 1, 2\}$.

One can generalize this construction to the general SU(N) case. In the iPEPS representation of the SU(N) singlet state, the required virtual bond dimension is increased by 1 and given by $D = D_{\mathrm{MPS}} + 1 = \binom{N}{\lfloor N/2 \rfloor} + 1$. For $N = 4$, the required bond dimension is $D = 7$ and the corresponding tensor elements of the iPEPS are summarized in Table II.

2. Tensor-network representation of the dimerized state

We prepare the dimerized initial state by placing the singlet pairs along the horizontal bonds connecting the sublattice sites A and B and those connecting the sublattice sites C and D in the 4×1 sublattice structure [see Fig. 3(b) and Fig. 5(b)]. For one singlet pair, we only use the physical bonds 0 and 1, corresponding to two out of four flavors of the SU(4) model. For the other singlet pair, we only use the physical bonds 2 and 3, corresponding to the remaining two flavors. Resulting tensor elements of the iPEPS are summarized in Table III. The required virtual bond dimension of this initial state in the iPEPS representation is $D = 3$ [70,71].

[1] C. Wu, J. P. Hu, and S. C. Zhang, Phys. Rev. Lett. **91**, 186402 (2003).

[2] C. Honerkamp and W. Hofstetter, Phys. Rev. Lett. **92**, 170403 (2004).

[3] M. A. Cazalilla, A. Ho, and M. Ueda, New J. Phys. **11**, 103033 (2009).

[4] A. V. Gorshkov, M. Hermele, V. Gurarie, C. Xu, P. S. Julienne, J. Ye, P. Zoller, E. Demler, M. D. Lukin, and A. Rey, Nat. Phys. **6**, 289 (2010).

[5] M. Hermele and V. Gurarie, Phys. Rev. B **84**, 174441 (2011).

[6] D. Yamamoto and K. Morita, Phys. Rev. Lett. **132**, 213401 (2024).

[7] S. Taie, R. Yamazaki, S. Sugawa, and Y. Takahashi, Nat. Phys. **8**, 825 (2012).

[8] Y. Kitaoka, T. Kobayashi, A. Kōda, H. Wakabayashi, Y. Niino, H. Yamakage, S. Taguchi, K. Amaya, K. Yamaura, M. Takano, A. Hirano, and R. Kanno, J. Phys. Soc. Jpn. **67**, 3703 (1998).

[9] F. Reynaud, D. Mertz, F. Celestini, J.-M. Debierre, A. M. Ghorayeb, P. Simon, A. Stepanov, J. Voiron, and C. Delmas, Phys. Rev. Lett. **86**, 3638 (2001).

[10] S. Nakatsuji, K. Kuga, K. Kimura, R. Satake, N. Katayama, E. Nishibori, H. Sawa, R. Ishii, M. Hagiwara, F. Bridges, T. U. Ito, W. Higemoto, Y. Karaki, M. Halim, A. A. Nugroho, J. A. Rodriguez-Rivera, M. A. Green, and C. Broholm, Science **336**, 559 (2012).

[11] J. A. Quilliam, F. Bert, E. Kermarrec, C. Payen, C. Guillot-Deudon, P. Bonville, C. Baines, H. Luetkens, and P. Mendels, Phys. Rev. Lett. **109**, 117203 (2012).

[12] A. Smerald and F. Mila, Phys. Rev. B **90**, 094422 (2014).

[13] K. I. Kugel, D. I. Khomskii, A. O. Sboychakov, and S. V. Streltsov, Phys. Rev. B **91**, 155125 (2015).

[14] M. G. Yamada, M. Oshikawa, and G. Jackeli, Phys. Rev. Lett. **121**, 097201 (2018).

[15] D. Greif, T. Uehlinger, G. Jotzu, L. Tarruell, and T. Esslinger, Science **340**, 1307 (2013).

[16] R. A. Hart, P. M. Duarte, T.-L. Yang, X. Liu, T. Paiva, E. Khatami, R. T. Scalettar, N. Trivedi, D. A. Huse, and R. G. Hulet, Nature (London) **519**, 211 (2015).

[17] A. Mazurenko, C. S. Chiu, G. Ji, M. F. Parsons, M. Kanász-Nagy, R. Schmidt, F. Grusdt, E. Demler, D. Greif, and M. Greiner, Nature (London) **545**, 462 (2017).

[18] H. Ozawa, S. Taie, Y. Takasu, and Y. Takahashi, Phys. Rev. Lett. **121**, 225303 (2018).

[19] H.-J. Shao, Y.-X. Wang, D.-Z. Zhu, Y.-S. Zhu, H.-N. Sun, S.-Y. Chen, C. Zhang, Z.-J. Fan, Y. Deng, X.-C. Yao, Y.-A. Chen, and J.-W. Pan, arXiv:2402.14605.

[20] S. Taie, E. Ibarra-García-Padilla, N. Nishizawa, Y. Takasu, Y. Kuno, H.-T. Wei, R. T. Scalettar, K. R. Hazzard, and Y. Takahashi, Nat. Phys. **18**, 1356 (2022).

[21] H. Tsunetsugu and M. Arikawa, J. Phys. Soc. Jpn. **75**, 083701 (2006).

[22] A. Läuchli, F. Mila, and K. Penc, Phys. Rev. Lett. **97**, 087205 (2006).

[23] D. Yamamoto, C. Suzuki, G. Marmorini, S. Okazaki, and N. Furukawa, Phys. Rev. Lett. **125**, 057204 (2020).

[24] T. A. Tóth, A. M. Läuchli, F. Mila, and K. Penc, Phys. Rev. Lett. **105**, 265301 (2010).

[25] Y.-W. Lee and M.-F. Yang, Phys. Rev. B **85**, 100402(R) (2012).

[26] H. H. Zhao, C. Xu, Q. N. Chen, Z. C. Wei, M. P. Qin, G. M. Zhang, and T. Xiang, Phys. Rev. B **85**, 134416 (2012).

[27] P. Corboz, M. Lajkó, K. Penc, F. Mila, and A. M. Läuchli, Phys. Rev. B **87**, 195113 (2013).

[28] D. P. Arovas, Phys. Rev. B **77**, 104404 (2008).

[29] P. Corboz, K. Penc, F. Mila, and A. M. Läuchli, Phys. Rev. B **86**, 041106(R) (2012).

[30] Y. Miyazaki, D. Yamamoto, G. Marmorini, and N. Furukawa, AIP Adv. **11**, 025202 (2021).
[31] Y. Miyazaki, G. Marmorini, N. Furukawa, and D. Yamamoto, J. Phys. Soc. Jpn. **91**, 073702 (2022).
[32] P. Corboz, A. M. Läuchli, K. Penc, M. Troyer, and F. Mila, Phys. Rev. Lett. **107**, 215301 (2011).
[33] Y. Q. Li, M. Ma, D. N. Shi, and F. C. Zhang, Phys. Rev. Lett. **81**, 3527 (1998).
[34] M. van den Bossche, F.-C. Zhang, and F. Mila, Eur. Phys. J. B **17**, 367 (2000).
[35] M. van den Bossche, P. Azaria, P. Lecheminant, and F. Mila, Phys. Rev. Lett. **86**, 4124 (2001).
[36] H.-H. Hung, Y. Wang, and C. Wu, Phys. Rev. B **84**, 054406 (2011).
[37] E. Szirmai and M. Lewenstein, Europhys. Lett. **93**, 66005 (2011).
[38] P. Corboz, M. Lajkó, A. M. Läuchli, K. Penc, and F. Mila, Phys. Rev. X **2**, 041013 (2012).
[39] M. Lajkó and K. Penc, Phys. Rev. B **87**, 224428 (2013).
[40] M. Mikkelsen and I. Danshita, Phys. Rev. A **107**, 043313 (2023).
[41] X.-J. Yu, S.-H. Shi, L. Xu, and Z.-X. Li, Phys. Rev. Lett. **132**, 036704 (2024).
[42] M. A. Martín-Delgado, M. Roncaglia, and G. Sierra, Phys. Rev. B **64**, 075117 (2001).
[43] F. Verstraete and J. I. Cirac, arXiv:cond-mat/0407066.
[44] F. Verstraete and J. I. Cirac, Phys. Rev. A **70**, 060302(R) (2004).
[45] F. Verstraete, V. Murg, and J. I. Cirac, Adv. Phys. **57**, 143 (2008).
[46] J. Jordan, R. Orús, G. Vidal, F. Verstraete, and J. I. Cirac, Phys. Rev. Lett. **101**, 250602 (2008).
[47] H. N. Phien, J. A. Bengua, H. D. Tuan, P. Corboz, and R. Orús, Phys. Rev. B **92**, 035142 (2015).
[48] R. Orús, Ann. Phys. **349**, 117 (2014).
[49] R. Orús, Nat. Rev. Phys. **1**, 538 (2019).
[50] Y. Hieida, K. Okunishi, and Y. Akutsu, New J. Phys. **1**, 7 (1999).
[51] K. Okunishi and T. Nishino, Prog. Theor. Phys. **103**, 541 (2000).
[52] T. Nishino, Y. Hieida, K. Okunishi, N. Maeshima, Y. Akutsu, and A. Gendiar, Prog. Theor. Phys. **105**, 409 (2001).
[53] N. Maeshima, Y. Hieida, Y. Akutsu, T. Nishino, and K. Okunishi, Phys. Rev. E **64**, 016705 (2001).
[54] Y. Nishio, N. Maeshima, A. Gendiar, and T. Nishino, arXiv:cond-mat/0401115.
[55] Y. Motoyama, T. Okubo, K. Yoshimi, S. Morita, T. Kato, and N. Kawashima, Comput. Phys. Commun. **279**, 108437 (2022).
[56] TeNeS: https://github.com/issp-center-dev/TeNeS.
[57] pTNS: https://github.com/TsuyoshiOkubo/pTNS.
[58] H. C. Jiang, Z. Y. Weng, and T. Xiang, Phys. Rev. Lett. **101**, 090603 (2008).
[59] T. Nishino and K. Okunishi, J. Phys. Soc. Jpn. **65**, 891 (1996).
[60] T. Nishino and K. Okunishi, J. Phys. Soc. Jpn. **66**, 3040 (1997).
[61] T. Nishino, T. Hikihara, K. Okunishi, and Y. Hieida, Intl. J. Mod. Phys. B **13**, 1 (1999).
[62] R. Orús and G. Vidal, Phys. Rev. B **80**, 094403 (2009).
[63] P. Corboz, J. Jordan, and G. Vidal, Phys. Rev. B **82**, 245119 (2010).
[64] P. Corboz, S. R. White, G. Vidal, and M. Troyer, Phys. Rev. B **84**, 041108(R) (2011).
[65] P. Corboz, T. M. Rice, and M. Troyer, Phys. Rev. Lett. **113**, 046402 (2014).
[66] S. Trotzky, Y.-A. Chen, U. Schnorrberger, P. Cheinet, and I. Bloch, Phys. Rev. Lett. **105**, 265303 (2010).
[67] B. Paredes and I. Bloch, Phys. Rev. A **77**, 023603 (2008).
[68] S. Nascimbène, Y.-A. Chen, M. Atala, M. Aidelsburger, S. Trotzky, B. Paredes, and I. Bloch, Phys. Rev. Lett. **108**, 205301 (2012).
[69] S. Wenzel and W. Janke, Phys. Rev. B **79**, 014410 (2009).
[70] F. Verstraete, M. M. Wolf, D. Perez-Garcia, and J. I. Cirac, Phys. Rev. Lett. **96**, 220601 (2006).
[71] N. Schuch, D. Poilblanc, J. I. Cirac, and D. Pérez-García, Phys. Rev. B **86**, 115108 (2012).